Journal of Materials Chemistry C

ROYAL SOCIETY OF CHEMISTRY

PAPER

View Article Online
View Journal | View Issue



Cite this: J. Mater. Chem. C, 2025, 13, 831

# Light-induced magnetic switching in a coumarin-based Tb single molecule magnet†

Elena Bartolomé, *[a] Ana Arauzo, *[b] Javier Luzón [c] and Laura Gasque [d]

We present the intriguing magneto-optical properties of the lanthanide complex [Tb(coum)$_3$(batho)]·[0.7EtOH], named **Tb–batho**, based on coum = 3-acetyl-4-hydroxylato-coumarin and batho = bathophenanthroline ligands. **Tb–batho** displays visible-range luminescence with a notable quantum yield (58%) upon sensitization of the "antenna" ligands. Employing a SQUID magnetometer equipped with a magneto-optic option, we conducted comprehensive *in situ* measurements of light-induced magnetization changes across varied magnetic fields, temperatures, and frequencies, utilizing light wavelengths ranging from 275 to 800 nm. A reversible magnetic modulation of magnetization is observed upon toggling the light "on" and "off," particularly pronounced at 380 nm excitation, resulting in a magnetization change $\Delta M$(off/on) = 0.376$\mu_B$ fu$^{-1}$ (*ca.* 42.6% of the magnetization) at 1.8 K and 1 kOe. Although **Tb–batho** exhibits field-induced single ion magnet (SIM) behavior, characterized by a thermally-activated process with an activation energy of $U_{eff}/k_B$ = 16.6 K @ 3 kOe and a slow direct process influenced by bottleneck effects, light irradiation does not noticeably alter its dynamic properties. All in all, **Tb–batho** emerges as a versatile multifunctional molecular material integrating SIM behavior, luminescence and light-induced magnetic switching, holding interest for diverse electronic applications, sensors, or quantum computing.

Received 24th July 2024,
Accepted 8th November 2024

DOI: 10.1039/d4tc03152k

rsc.li/materials-c



## 1. Introduction

In recent years, the appeal of smart materials endowed with multifunctional and controllable properties has significantly grown due to their broad applicability across diverse fields. Among them, metal–organic materials are particularly attractive because their chemical fabrication facilitates reproducibility, miniaturization, and scalability—critical aspects in preparing nanodevices—and allows for the tunability of properties. Multifunctional molecular magnetic materials, characterized by unique functionalities in tandem with magnetic properties, such as luminescence, microporosity, conductivity, and chirality, have garnered interest for various applications, including switching, sensing, spintronics,[1] gas separation,[2] catalysis,[3] or biomedicine.[4,5] A particularly promising avenue is the exploration of molecular materials that combine both luminescence with magnetic properties, opening up new opportunities in applications such as information storage and processing, sensing and bioimaging.[6] Moreover, the ability to control the magnetization though optical stimulation is an attractive property for different applications, and has been searched in different types of inorganic[7,8] and organic materials.[9] Among them, extensive investigation has been done on optical-driven magnetization changes in transition-metal compounds, Fe–Co Prussian blue analogues and CN-bridging compounds, light-induced excited spin state trapping (LIESST) compounds, composites, and more recently, topological spin switching has been achieved in 2D van der Waals magnets.[10]

Lanthanide ions hold unique electronic, optical, and magnetic properties derived from 4f orbitals, making them excellent candidates for the development of stimuli-responsive molecular materials. Indeed, trivalent lanthanides ($Ln^{3+}$), characterized by large unquenched orbital moments and high magnetic anisotropy, are particularly suited for designing single-molecule magnets (SMMs).[11–13] Recent advancements have led to the creation of lanthanide-based single-ion magnets (SIMs) with activation energies ($U_{eff}$) around 2000 K and blocking temperatures exceeding 80 K.[14] Simultaneously, Ln(III)-based materials exhibit exceptional luminescent properties, featuring intense, narrow-banded, and long-lived emission bands spanning the visible and near-infrared spectrum,[15–18] although luminescence typically requires sensitization through a harvesting "antenna" ligand, given the

[a] Institut de Ciència de Materials de Barcelona (ICMAB-CSIC), Campus UAB, 08193-Bellaterra, Barcelona, Spain. E-mail: ebartolome@icmab.es
[b] Instituto de Nanociencia y Materiales de Aragón (INMA), CSIC-Universidad de Zaragoza, and Departamento de Física de la Materia Condensada, 50009 Zaragoza, Spain. E-mail: aarauzo@unizar.es
[c] Centro Universitario de Defensa (CUD), Universidad de Zaragoza, Spain
[d] Facultad de Química, Universidad Nacional Autónoma de México, Avenida Universidad 3000, CDMX 04510, Mexico

† Electronic supplementary information (ESI) available: Crystal structure of **Tb-batho**; relaxation time as function of 1/$T$ and $H$; *ab initio* calculated energy levels. See DOI: https://doi.org/10.1039/d4tc03152k

inherent weakness of direct excitation of Ln ions. The literature extensively reports on the SMM and luminescence properties of $Ln^{3+}$ compounds with various dimensionalities. These include: 0D SIM,[19–30] dinuclear compounds,[31–39] SMM clusters,[40–46] 1D polymeric compounds,[47–53] 2D metal–organic compounds (MOFs),[54] and 3D MOFs.[55] However, among these only a limited number of complexes truly exhibit bifunctionality, demonstrating both SMM behavior and photoluminescence.[6,56–58] The design of the ligands to achieve this bifunctionality plays a crucial role, influencing the coordination environment, relevant for magnetic relaxation, while facilitating luminescence sensitization.[57,59–62]

On the other hand, significant efforts have been made in recent years towards achieving switchable Ln-based SMMs *via* external stimuli, encompassing physical influences such as light, temperature, pressure, and electric potential, as well as chemical stimuli like redox reactions, pH responsiveness, or guest exchange. The primary strategies for designing switchable Ln-SMMs involve methods that achieve reversible single-crystal to single-crystal (SC–SC) structural transformations, including solvato switching of Ln-SMMs[63,64] (particularly within MOFs[65–67]), proton switching,[68–70] redox switching (based on either ligand-centered,[71–74] or metal-centered[75,76] redox-activity) and photo-switching. Light irradiation is a preferred stimulus due to its convenient and rapid response, enabling dynamic remote control.

The most widely employed strategy for designing photoswitchable Ln-SMMs has been the use of photocrhomic ligands, which facilitate a light-driven reversible transformation between two isomeric forms. However, a major challenge to this approach is that the light-driven changes hardly affect the first coordination environment of the Ln ions, which ultimately influences the magnetic anisotropy and SMM behavior. For instance, in Ln-SMMs based on DTE, the light-induced cyclo-isomerization produced insufficient structural changes for significant magnetic modulation.[77] Other photoactive ligands, including 1,2-bis(4-pyridyl)ethene (bpe), anthracene (or its derivatives),[78–80] and spiropyran-merocyanines[81] have been employed to construct photo-responsive Ln-SMMs; however, despite achieving SC–SC transformations and modulation of the SMM behavior, these processes were not reversible.

In a few cases, reversible SC–SC transformations accompanied by changes in SMM properties have been reported. In a photocrhomic chain of $[Dy(Tp^{py})F(pyridine)_2]PF_6$ ($Tp^{py}$ = tris(3-(2-pyridyl)pyrazolyl)hydroborate) reversible SC–SC isomerization occurred upon on/off visible irradiation, albeit with only partial conversion towards the closed form; both isomeric forms displayed identical slow relaxation of magnetization, although the relaxation time for quantum tunneling of the magnetization (QTM) was reduced for the open form with respect to the open form, leading to a narrower hysteresis loop.[82] Following a different approach, a radical-actuated on/off SMM was demonstrated in chain compounds $[Dy_3(HEDP_3^{-})_3(HEDP_2^{-})_3]\cdot 2TPT_3^{+}\cdot HEDP\cdot 10H_2O$. HEDP = hydroxyethylidene diphosphonate; TPT = (2,4,6-tri(4-pyridyl)-1,3,5-triazine). These crystals, when illuminated by UV light, turned blue and returned to the initial colorless state upon heating to 100 °C for 0.5 h. The process involved photoinduced photoelectron transfer (PET) from HEDP-Dy(III) chains to TPT, leading to SMM behavior attributed to the large anisotropy of Dy(III) ions and the strong ferromagnetic coupling between the photogenerated anionic $O^{\bullet}$ radicals and Dy(III) ions.[83] In another example, the anthracene-based complex $Dy(depma)(NO_3)_3(hmpa)_2$ (depma = 9-diethylphosphonomethylanthracene, hmpa = hexamethylphosphoramide) exhibited a reversible SC–SC transformation, resulting in a change in magneto-optic properties from SIM behavior with yellow-green emission to SMM with blue-white emission upon irradiation at 365 nm for 0.5 h. The reverse transformation occurred upon heating the dinuclear compound at 100 °C in air.[84] It is important to note that in all the previously mentioned examples, "on" switching of the SMM required prolonged irradiation, while the reversible "off" transformation was not induced optically but rather thermally.

In addition to these efforts to manipulate SMM memories using light, there is a growing interest in employing optical methods to drive molecular qubits for quantum computing, as a rapid and sensitive alternative to microwave control.[85] Recently, qubit initialization of a $[Eu^{2+}]$ molecule through optical-induced spin polarization was reported,[86] and the optical readout of Ln-based qubits has been theoretically proposed.[87] The development of high performing bifunctional molecules and the understanding of magneto-optical coupling is a pre-requirement to advance in all the above described challenges.

In our previous research, we demonstrated the effectiveness of a chelating coumarin-derived antenna ligand to sensitize $[Ln(Coum)_3(EtOH)(H_2O)]EtOH$ in solid state for all Ln ions.[88] Coumarins, a family of 1,2-benzopyrones widely found in plants, exhibit remarkable optical properties. Substituting some of the coordination ligands with aromatic diimine (batho = bathophenanthroline or 4,7-diphenyl-1,10-phenanthroline[89]) or (phen = 1,10 phenanthroline) chromophores resulted in compounds $[Ln(coum)_3(phen)(H_2O)_x]\cdot yH_2O$ ($x = 0, 1$; $0 \leq y \leq 1.5$) and $[Ln(coum)_3(batho)]\cdot 0.7EtOH$ (Ln = Eu, Tb, Dy, Tm) showcasing interesting magnetic and photoluminescent properties. Specifically, Dy and Tb compounds exhibited SIM behavior and remarkably high luminescence quantum yields (QY), of 65–76–58% for **Tb–coum**, **phen**, **batho** analogues. Notably, the last two compounds displayed values of the bifunctional figure of merit $\eta_{SMM\text{-}QY} = Q_{Ln}^{ligand}\cdot U_{eff}$ (the product of QY and the activation energy for spin reversal) reaching 968.6% K (889.2% K) for **Tb–batho** (**Tb-phen**), above all reported bifunctional Tb compounds in the literature.[50,90–93]

In this work, we report our investigation of the optical modulation of the magnetic properties of **Tb–batho** single molecule magnet. *In situ* measurement of the magnetization changes induced by an external light source was achieved through the use of a magnetometer equipped with a Magneto-Optic option.

## 2. Materials and methods

### Synthesis

Lanthanide nitrate hydrates, 1,10-phenanthroline, bathophenanthroline, $CH_3ONa$ solution and all solvents were purchased

 

from Sigma-Aldrich and used without further purification. Ligand Hcoum (3-acetyl-4-hydroxy-2-benzopyrone) was synthesized as described previously.[88] **Tb–batho** was prepared by isolating first the corresponding $Tb(coum)_3$ complex obtained by mixing in ethanol 1 mmol of the lanthanide nitrate with 3 mmol of Hcoum and 3 mmol $CH_3ONa$ from a 0.5 N methanolic solution. After stirring at 60 °C for three hours, precipitating and drying this product, one equivalent of bathophenanthroline was added in ethanolic solution and the mixture stirred at 60 °C for 48 hours. Ethanol was partially evaporated, and water was added to precipitate the product, which was then filtered and dried. Single crystals suitable for X-ray diffraction were obtained by slow evaporation of the products dissolved in $CH_2Cl_2$–EtOH.

### Tb–batho

Yield = 96% MALDI-TOF (*m*/*z*) positive ion: 897.1 $[Tb(coum)_2(batho)^+]$; negative ion 767 $[Tb(coum)_3\text{-}H]^-$. Elemental analysis calc. for $Tb(coum)_3(batho)\cdot EtOH$ (%): C: 61.44, H: 3.73, N: 2.47. Experimental: C: 61.53, H 3.63, N: 2.51. IR-ATR ($cm^{-1}$) IR: 1708 ($\nu$C=O lactone), 1609 ($\nu$C=O $COCH_3$), 1466 ($\delta_{as}$ $CH_3$), 1389 ($\delta_s$ $CH_3$), 837, 704 (batho rings).

### Solid state luminescent measurements

Photoluminescence emission and excitation spectra were measured using a Fluorolog FL-1057 Jobin Ybon HORIBA spectrofluorometer. Quantum yields (QY) of samples in solid state were measured under excitation wavelengths ranging from $\lambda_{exc}$ = 275–415 nm at 300 K using a Hamamatsu absolute PL quantum yield spectrometer C11347 (Hamamatsu quantaurus QY) equipped with an integrating sphere.

### Magnetic measurements

Characterization of powdered samples embedded in Daphne oil to prevent grain orientation was performed in the temperature range 1.8 to 300 K using a Quantum Design MPMS3 SQUID equipped with a 50 kOe magnet. Ac susceptibility measurements in the range between 1.8–9.0 K, at $H_{ac}$ = 4.1 Oe, $H_{dc}$ = 0–25 kOe in the range of frequencies between $f$ = 0.1–1000 Hz were determined in the same SQUID magnetometer. Additional measurements in the expanded range $f$ = 10–10 kHz were performed in a Quantum Design PPMS.

Optically-driven magnetic switching experiments were performed in a Quantum Design MPMS3 SQUID provided with a magneto-optical (MO) option. Thin, disc-shaped pellets were prepared (Pellet 1: diameter $D \approx 2.5$ mm, thickness $t \approx 0.05$ mm; Pellet 2: $D \approx 2.5$ mm, $t \approx 1$ mm; Pellet 3: $D \approx 2.0$ mm, $t \approx 1$ mm), and were placed in the quartz cavity inside the MO Fiber Optic Sample Holder (FOSH) of the SQUID. For the experiments, different sources of light were used: (i) a LED lamp of constant $\lambda_{exc}$ = 275 nm, (ii) a 75 W XENON lamp combined with a low-pass filter ($\lambda_{exc} < 450$ nm), and (iii) a 100 W XENON TLS120Xe Quantum Design light source, with tunable monochromatic wavelength between 280 nm and 1100 nm, and a fixed bandwidth of 20 nm.[94]

*Ab initio* calculations were performed on the **Tb–batho** molecule using the CASPT2/RASSI-SO[95] method as implemented in the MOLCAS 8.2[96] quantum chemistry package. All the atoms were represented by basis sets of atomic natural orbitals from the ANO RCC library:[97] the VQZP basis set for the Tb ion, the VTZP one for the O, N and C atoms in the first, second and third shells of atoms around the Tb ion and the VDZ one for all the other atoms. The chosen CASSCF active space included the seven 4f Tb orbitals containing 8 electrons: CASSCF(8,7). After preliminary calculations with a larger number of states, the final state-averaged CASSCF calculations included all the states in the range from 0 to 60 000 $cm^{-1}$ (the 7 septets, 105 quintets, 112 triplets, 0 singlets).

## 3. Results

The synthesis, structure and magnetic properties of non-irradiated $[Tb(coum)_3(batho)]\cdot 0.7EtOH$ (named **Tb–batho**, CCDC-2013258) were previously described.[98] The crystal unit cell is triclinic (space group $P\bar{1}$ (2)), with cell parameters $a$ = 11.6630(4) Å, $b$ = 13.2469(6) Å, $c$ = 18.3330(8) Å, $\alpha$ = 78.553(3)°, $\beta$ = 76.079(3)°, $\gamma$ =

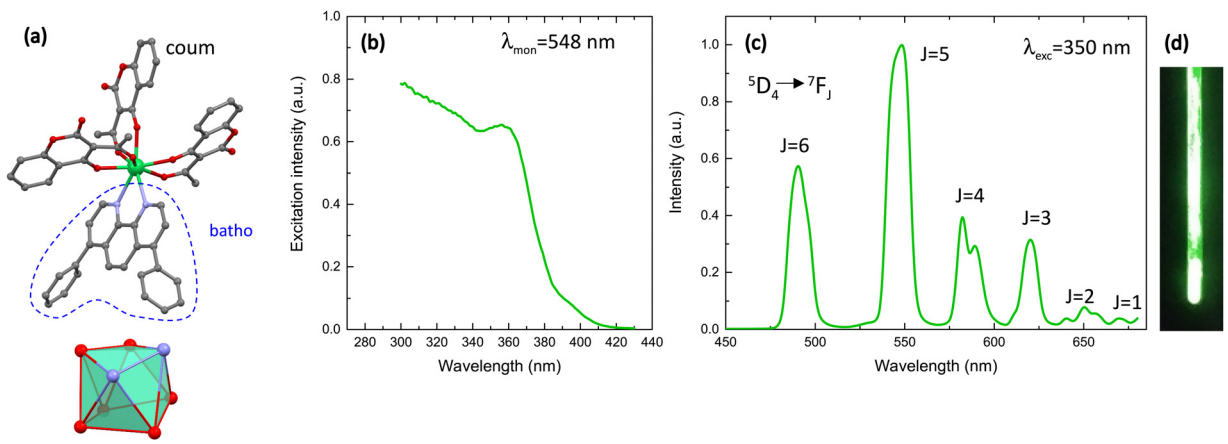


Fig. 1 (a) Structure of **Tb–batho**. Colour code: Tb (green), O(red), N (blue), C (grey). H atoms are omitted for clarity. Below, detail of the coordination polyhedron; (b) excitation spectrum, monitorized at $\lambda_{mon}$ = 548 nm, and (c) emission spectrum under an excitation wavelength of $\lambda_{ex}$ = 350 nm of a solid sample of **Tb–batho** at room temperature (adapted from ref. 98); (d) visible emission under UV light.

68.680(3)°, (see Table S1, ESI† for details). The molecular structure of the **Tb–batho** complex (Fig. 1, left) is formed by three independent bidentate deprotonated coumarin ions $(C_{11}H_7O_4)^-$, which bond through their acetyl and hydroxy O atoms to the Tb site, thereby stabilizing 6-membered metallacycles. The coum ligand O–Tb–O bite angle is approximately 68°. Additionally, a batho ligand (bathophenanthroline or 4,7-diphenyl-1,10-phenanthroline) in bidentate mode bonds through its two N atoms to the Tb ion, with a bite angle of 63° for the N–Tb–N angle. The $Tb^{3+}$ ion is thus octa-coordinated by two adjacent N ions, provided by the batho ligand, and six O ions from the three coum ligands. The coordination polyhedron adopts a distorted square antiprism geometry (polyhedral symbol: SAPR-8,[99] point group of the uniform polyhedron: $D_{4d}$), and has the square faces presenting a butterfly shape.

The magnetization as a function of the magnetic field $M(H)$, measured at $T$ = 1.8 K, reached a saturation magnetization value of $M_{sat} = 4.8\mu_B$ fu$^{-1}$, close to the expected value for $Tb^{3+}$ ions with $g_z^* = 18$, within a $S^* = 1/2$ effective-spin model. The temperature dependence of the susceptibility times de temperature product, $\chi T(T)$, measured under 1 kOe, reached a saturation value at 300 K of 11.1 emu K mol$^{-1}$, consistent with the free-ion theoretical prediction,[100] $\chi T = g_J^2 J(J+1)/8$ of 11.8 emu K mol$^{-1}$ for $Tb^{3+}$ ($^7F_6$, $g_J$ = 3/2). By decreasing the temperature, the $\chi T$ value smoothly decreased from room temperature to 11 K, and then more abruptly until reaching 9.3 emu K mol$^{-1}$ at 1.8 K. This behavior was attributed to the progressive thermal depopulation of the excited $M_J$ sublevels. The dynamic magnetization, characterized by ac susceptibility measurements as a function of frequency, temperature and dc magnetic field, revealed that **Tb–batho** does not show out-of-phase ($\chi''$) signal in the absence of field below 5 K, indicating a significant QTM channel, preventing slow spin relaxation. $\chi''(f, H, 2\text{ K})$ measurements and $\chi''(f, T)$ measurements at the optimum field (3 kOe) optimizing the $\chi''$ intensity revealed the presence of a low frequency (LF) peak at *ca.* 1 Hz, associated to a direct slow relaxation mechanism, and a higher frequency (HF) peak which afforded a thermal activation Orbach fitting, $\tau = \tau_0 \exp(U_{eff}/k_BT)$, with an activation energy of $U_{eff}/k_B$ = 16.6 K ($\tau_0 = 3.3 \times 10^{-7}$ s).

The luminescent properties measured for **Tb–batho** in the solid state are summarized in Fig. 1(b) and (d). The excitation spectrum of this compound presents a band at approximately 360 nm, associated to harvesting of the coum and batho ligands (Fig. 1(b)). The emission spectrum upon ligand excitation displays four characteristic bands (with largest peak at 546 nm), corresponding to the $^5D_4 \rightarrow {}^7F_J$ ($J$ = 6, 5, 4, 3) transitions to the ground state multiplet of Tb(III) ion (Fig. 1(c)). The measured quantum yield upon ligand excitation was notably large, $Q_{Tb}^{ligand}$ = 58%. As mentioned in the introduction, the achieved bifunctional figure of merit for this compound was remarkably high ($\eta_{SMM\text{-}QY} = Q_{Ln}^{ligand} \cdot U_{eff} = 968.6\%$ K), compared to previously reported Tb compounds. Therefore, we considered **Tb–batho** to be a suitable choice for our subsequent studies of magnetization modulation under light switching.

In the present study, we used thin, disc-shaped pellets of the **Tb–batho** sample, that were mounted onto the quartz sample holder within the fiber optic sample holder (FOSH) of a MPMS3 SQUID magnetometer equipped with the magneto-optic measurement option.[101] This set up enabled measurement of dc and ac magnetic properties as a function of temperature (1.8–300 K), magnetic field (0–70 kOe) and frequency (0.1–1000 Hz), while illuminating the sample with light of different wavelengths between 280–800 nm.

To begin, we measured the magnetization as a function of the time, at $T$ = 10 K under an applied magnetic field of $H$ = 1 kOe, as the light was alternatively switched "off/on/off/on". Fig. 2(a) shows the results of this experiment, for different values of the incident light wavelength, ranging between 280 nm and 650 nm. Clearly, "off/on" switching of the light produces a corresponding reduction in the magnetization, $\Delta M$(off/on), followed by a reversible "on/off" response. The down turn of the magnetization is produced within <12 s after switching "on" the light. The magnitude of the magnetization change $\Delta M$(off/on) depends on the wavelength of the irradiating light, as seen in Fig. 2(a), reaching a maximum of $\Delta M$(off/on) = $0.0108\mu_B$ fu$^{-1}$ (6.2% of the magnetization at 10 K) under $\lambda$ = 380 nm light. That is, maximum magnetization modulation is observed under approximately the same energy necessary to optimally sensitize the ligand.

Using the optimum irradiation wavelength of 380 nm, we conducted magnetization *versus* time "off/on" experiments at various temperatures, as shown in Fig. 2(b). Fig. 2(c) illustrates the temperature dependence of $\Delta M$(off/on) from 1.8 K to 10 K. At the lowest measured temperature, $T$ = 1.8 K, the magnetization change achieves a substantial value of $\Delta M$(off/on) = $0.376\mu_B$ fu$^{-1}$ (42.6% of the magnetization at 1.8 K).

It is noted that this light-induced decrease of magnetization is not accompanied by a detectable sample heating: throughout the "off/on" switching, the sample temperature monitored by a nearby thermometer remained constant within the experimental noise, within <0.005 K at 1.8 K (Fig. 2(d)). Moreover, the maximum magnetization change does not correlate with the maximum energy of the lamp source tested (250 nm), nor with the lamp power, which is maximum for a wavelength of 470 nm.[94]

To investigate the influence of the applied dc magnetic field on the light-induced magnetization change, we measured the field-dependence of the magnetization, $M(H)$, with the light switched off and on (380 nm) at $T$ = 1.8 K and 10 K (Fig. 3(a)). The difference between the two curves, denoted $\Delta M$(off/on)($H$) and depicted in Fig. 3(b), reveals that the light-induced change of magnetization peaks at 5 kOe (~20 kOe) at 1.8 K (10 K) at this wavelength. The magnetization change observed at 1 kOe coincides with the value obtained through $M$(time) "off/on" switching experiments.

A similar light-induced magnetic response was reproduced using a second, thicker pellet, as shown in the ESI† (S2). In this case, however, the maximum light-induced magnetization change at 1.8 K was only 3%, which we attribute to a partial contribution of the sample to the effect due to the increased thickness.

Finally, we discuss the results of light irradiation on magnetization dynamics. Firstly, we carried out $M(H)$

 

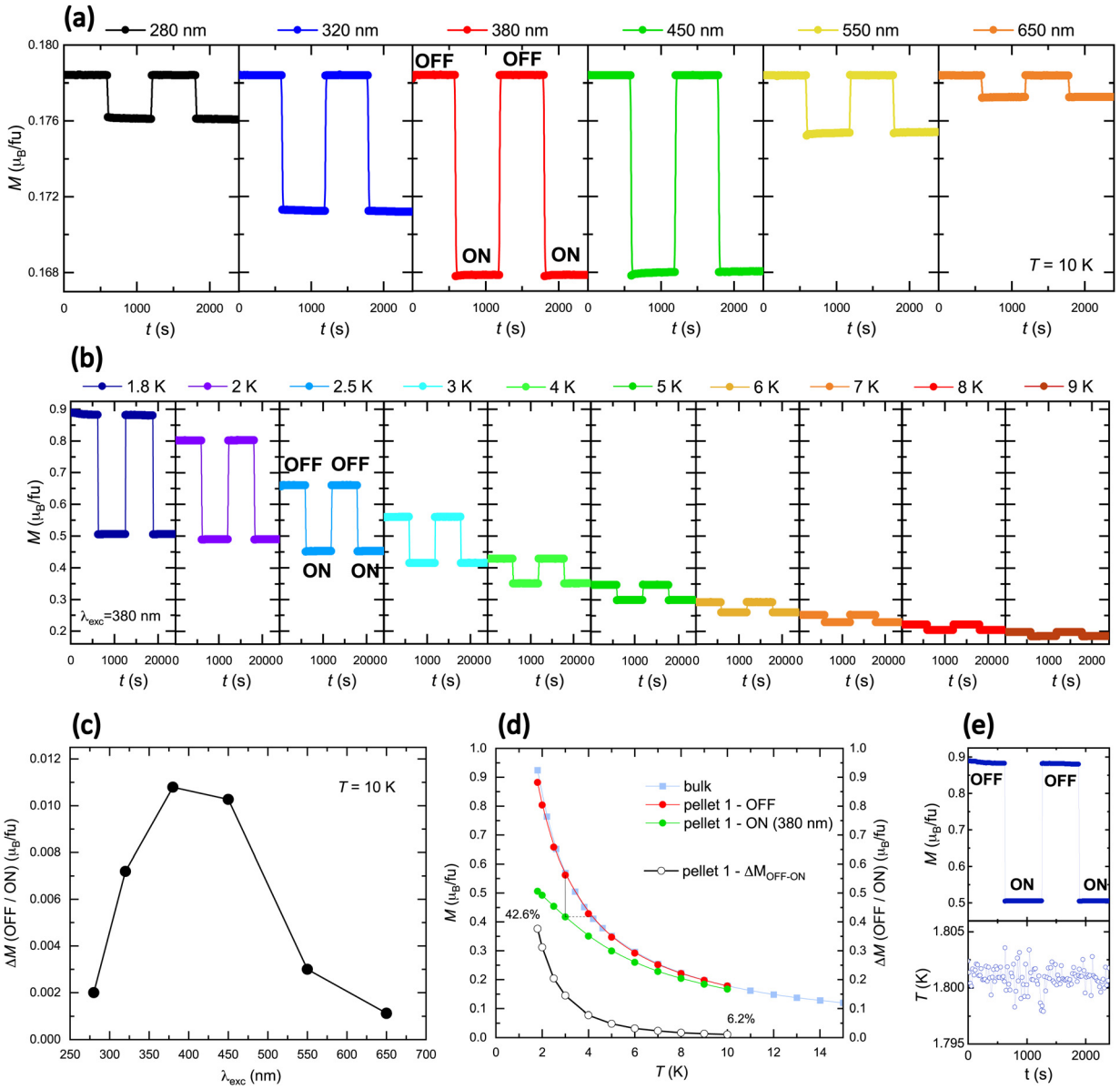


Fig. 2 (a) Magnetization as a function of time, $M(t)$, of **Tb–batho** at $T$ = 10 K, $H$ = 1 kOe, as the lamp is alternatively switched off/on/off/on, for different values of the incident light wavelength between 280 nm and 650 nm; (b) $M(t)$ off/on experiments (incident light of 380 nm) at different temperatures between 1.8 K and 9 K; (c) magnetization change between the off and on value as a function of the incident light wavelength, $\Delta M$(off/on) at 10 K, for an applied field of $H$ = 1 kOe; (d) magnetization as a function of the temperature with the light switched off and on and $\Delta M$(off/on) ($T$) (under $\lambda$ = 380 nm light) at $H$ = 1 kOe, and $M(T)$ previously reported for powdered sample; (d) thermometer temperature monitored during the off/on experiments (set $T$ = 1.8 K, $\lambda$ = 380 nm). Measurements conducted on pellet 1.

measurements on the non-irradiated, disc-shaped sampled placed in the magneto-optical FOSH holder.

Fig. 4(a) shows the $M(H)$ cycles measured at $T$ = 1.8 K while continuously ramping the magnetic field between 0 and 20 kOe, for different constant values of the field change rate. A "butterfly-like" magnetization cycle is observed for the largest ramp rate (700 Oe $s^{-1}$), which is typical of systems with SMM behavior, when the relaxing spins are unable to follow up the rapid changes of externally applied field. The $M(H)$ cycle progressively closes for smaller ramp rates, and at 50 Oe $s^{-1}$, the magnetization practically coincides with the curve measured in equilibrium.[98]

In Fig. 4(b), the $M(H)$ cycle measured at the highest rate, 700 Oe $s^{-1}$, is presented at three different temperatures. The opening of the "butterfly-like" cycle diminishes with increasing temperature, and is imperceptible at 10 K. The observation of these slow relaxation effects aligns with the previously reported existence of a very slow magnetic relaxation process, as determined from previous ac susceptibility measurements conducted on a powdered sample.[98] The relaxation time of this low-frequency process (LF), with a relaxation time $\tau_{LF} \sim 0.1$ s, very weakly dependent on the temperature and magnetic field, was linked to a direct process.[98] The second relaxation process observed in **Tb–batho**, attributed to

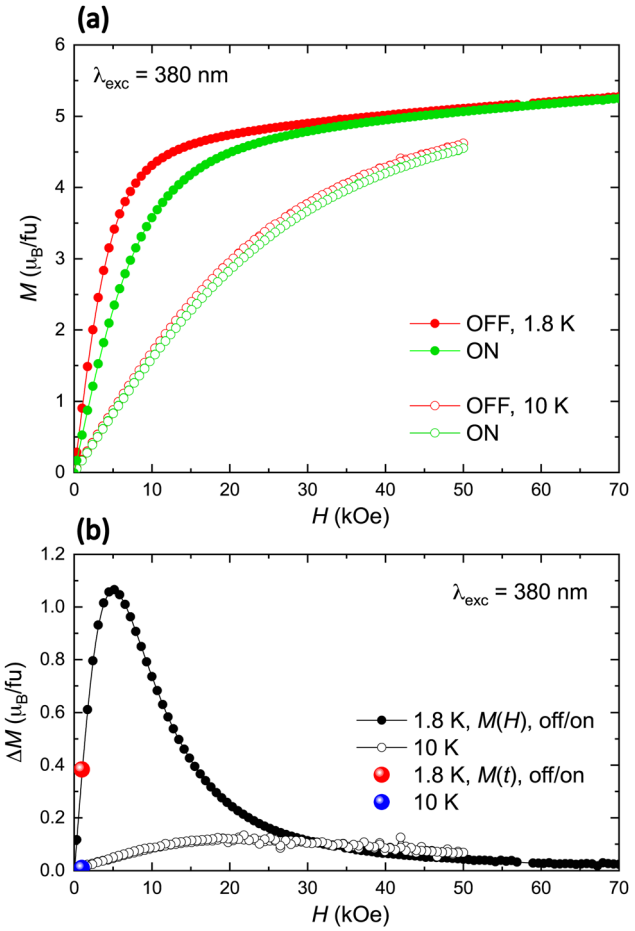


Fig. 3 (a) Field dependence of the magnetization at $T$ = 1.8 K and 10 K with the lamp switched off and on ($\lambda$ = 380 nm) obtained for pellet 1; (b) magnetization change between off/on (380 nm) as a function of magnetic field, obtained from $M(H)$ and $M$(time) experiments at 1.8 K and 10 K.

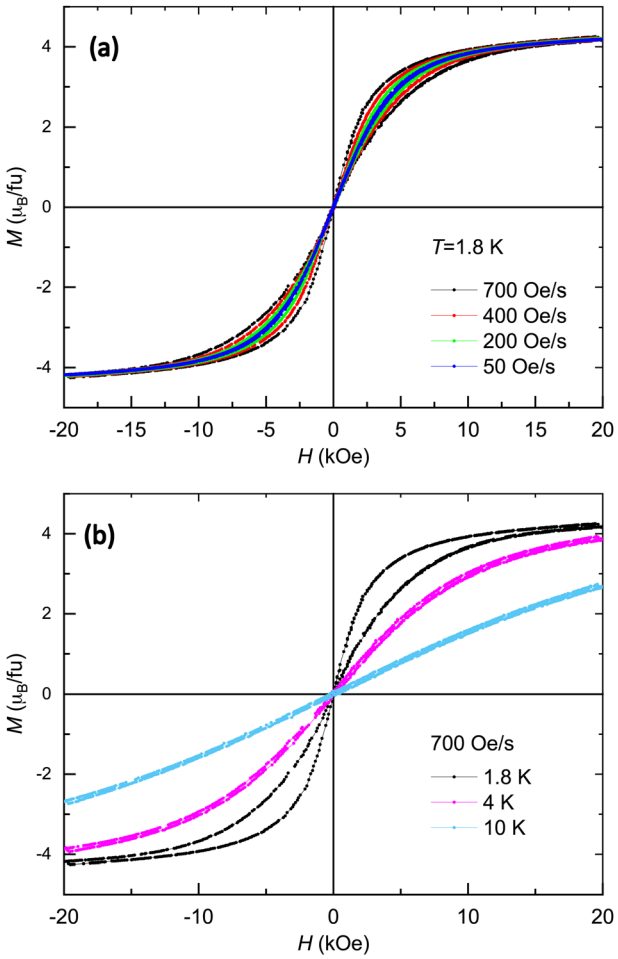


Fig. 4 (a) Magnetization as a function of applied magnetic field, $M(H)$, for a non-irradiated powdered sample of **Tb–batho** at $T$ = 1.8 K, where the field was swept at different rates (50 Oe $s^{-1}$, 200 Oe $s^{-1}$, 400 Oe $s^{-1}$, 700 Oe $s^{-1}$); (b) $M(H)$ measured by sweeping the magnetic field at 700 Oe $s^{-1}$, at different temperatures: 1.8 K, 4 K, 10 K.

thermally-activated SIM behavior ($U_{eff}/k_B$ = 16.6 K, $\tau_0$ = 3.3 × $10^{-7}$ s) transitioning to QTM with $\tau_{QT} \approx 10^{-5}$ s at low temperatures, was observed at very high frequencies >10 kHz, beyond the range of the current magnetometer (see Fig. S1, ESI†).

To investigate the impact of light irradiation on SIM behavior, we conducted ac susceptibility at 1.8 K and 3 kOe on a disc-shaped sample mounted in the SQUID with magneto-optical option, with the light turned "off" and "on" (Fig. 5). Two distinct samples were analyzed: a 2.5 mm-diameter disc, illuminated by a xenon lamp with a low-pass filter ($\lambda$ < 450 nm) (Fig. 5(b)), and a smaller approximately 2 mm-diameter fragment, irradiated with LED light at 275 nm (Fig. 5(a)).

For the larger disc, the $\chi''(f)$ data, both with the light "off" and "on", exhibit a peak at low frequency (~20 Hz) (Fig. 5(b)). Conversely, in the case of the smaller disc, this $\chi''$ peak shifts to higher frequencies (>1000 Hz) (Fig. 5(a)). This effect can be explained considering that this low-frequency relaxation process is associated to a direct process, often affected by bottleneck effects.[54,102–107] These effects occur when spins cannot relax sufficiently fast due to poor thermal contact with the bath, so the phenomenon is severely impacted by gas pressure conditions[108,109] and/or sample embedding, size and shape.[110,111] In our study, the bottleneck effect appears more pronounced in the powdered sample embedded in Daphne oil compared to the large pellet sample, and the effect weakens as the size of the pellet sample decreases. However, no significant change in the $\chi''$ signal is observed with the light switched "on" or "off".

In the final section of this article, we delve into the origin of the observed light-induced magneto-switching. Let's begin by examining the energy level scheme and energy transfer (ET) mechanism derived from luminescent measurements at room $T$ for **Tb–batho** (Fig. 6(a)). The sensitization mechanism involves the initial excitation of the molecule to states $S_1$, $S_2$, $S_n$ of the ligands, followed by electron relaxation by system intercrossing to available triplet states of the coumarin ($T_n$), an internal conversion to the lowest triplet state ($T_1$) of the ancillary ligand, an energy transfer to the Tb(III) lowest emitting level $^5D_4$ and, finally, radiative emission to the $^7F_J$ ($J$ = 0–6) levels. The energy difference between the ligand's $T_1$ and the

 

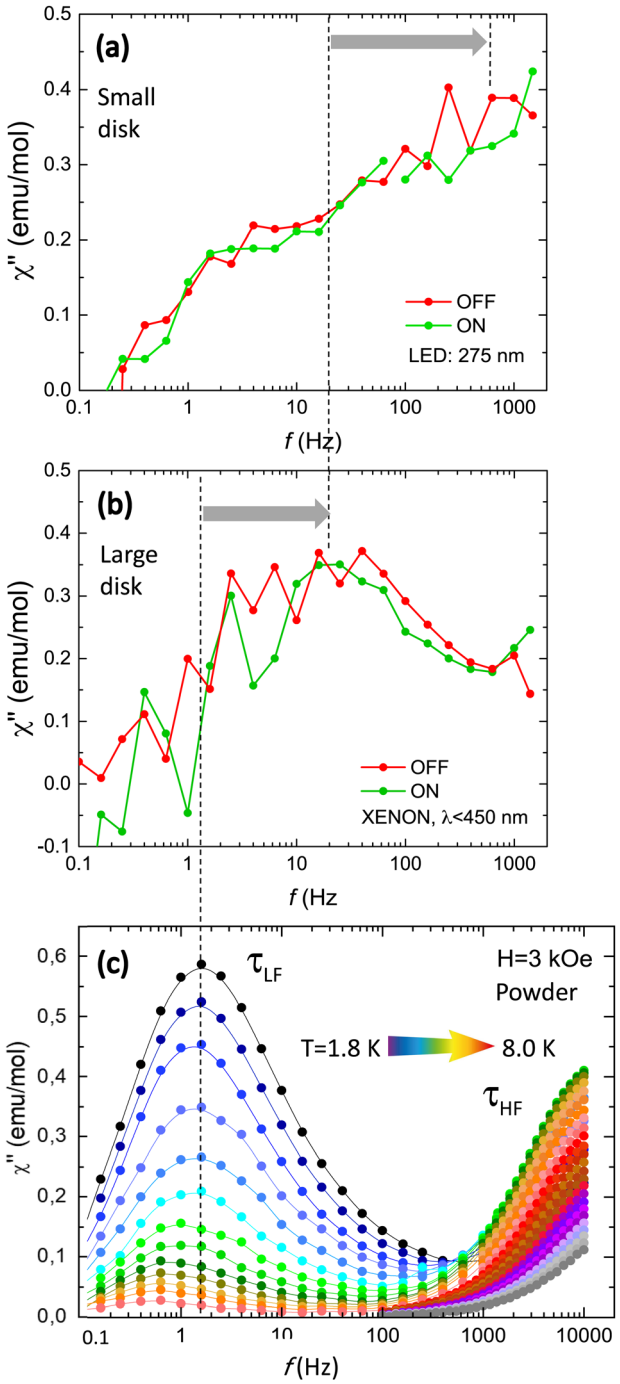


Fig. 5 Imaginary susceptibility as a function of the frequency of **Tb–batho** measured at $H$ = 3 kOe: (a) small disc sample (~2 mm-diameter, pellet 3), at $T$ = 1.8 K, with light on (LED lamp, $\lambda$ = 275 nm) and off; (b) larger disc sample (2.5 mm-diameter, pellet 2), at $T$ = 2 K, with light on (xenon lamp with filter $\lambda$ < 450 nm) and off; (c) for a non-irradiated powdered sample, at different temperatures between $T$ = 1.8–9 K.

Ln(III) emitting ligand, $\Delta E[T_1(\text{lig}) - \text{Tb}(^5D_4)]$, is generally regarded as the most relevant parameter dictating efficient ligand-to-metal ET. For the two ligands in **Tb–batho**, the $T_1$ triplet states lie at 24 570 (coum), and 20 900 (batho) $cm^{-1}$, positioning $\Delta E[T_1(\text{ligand})\text{-Tb}(^5D_4)]$ within the ideal range for achieving optimum QY for the coum ligand, but falling significantly below for batho. Nevertheless, the QY of **Tb–batho** is large (58%), and only slightly lower than that of the **Tb–coum** complex incorporating solely coumarin antenna ligands (65%). This suggests that in **Tb–batho**, the coumarin ligands play the main role as sensitizers, while the batho ligand modulates the emission by reducing the QY, possibly due to some back energy transfer (BET), and provoking a decrease in the emission decay lifetime (from $\tau_{obs}^{Tb}$ = 585 μs in **Tb–coum** to 465 μs in **Tb–batho**).

To gain further insight into the observed magneto-optical behavior, we calculated by *ab initio* the energy levels of the ligand-field split $^7F_6$ ($J$ = 0,1,2,3,4,5,6) and $^5D_4$ multiplets of Tb(III) in **Tb–batho** (Table S2, ESI†). The energy levels of the ground-state multiplet, $^7F_6$, and first excited multiplet, $^5D_4$, are represented in Fig. 6(b). Using the easy axis of magnetization (EAM) as the quantization axis, the composition of the corresponding 13 states,$\{|\xi_i|\}$, of $^7F_6$ in terms of the $J_z$ eigenstates has been obtained (Table S3, ESI†). The ground state, $|\xi_0\rangle = \sum_{M=-J}^{J} C^0_{J,M_J}|J, M_J\rangle$, is primarily composed of state $|J, M_J\rangle = |6, \pm6\rangle$ with some mixture from $|6, \pm5\rangle$. The first excited state of this multiplet, $|\xi_1\rangle = \sum_{M=-J}^{J} C^1_{J,M_J}|J, M_J\rangle$, is separated by a small energy gap of $\Delta/k_B$ = 0.143 K from $|\xi_0\rangle$. Therefore, the ground state can be considered as a non-Kramers "quasi-doublet", well separated from the next levels of the multiplet.[112] On the other hand, the lowest level of the $^5D_4$ multiplet is predominantly composed of the $|4,+4\rangle$ and the $|4,-4\rangle$ $J_z$ eigenstates, and is separated by a small gap ($\Delta'/k_B$ = 0.664 K) from the next level, forming an excited "quasi-doublet" (see Fig. 6(b)). At low temperatures, within an effective spin $S^*$ = 1/2 model, we can consider only the fundamental quasi-doublet of each multiplet, which will be split by the Zeeman effect under the application of a magnetic field.

In the absence of light irradiation, the sample magnetization originates solely from the population of the ground state. However, upon light pumping, the excited state can become (partially) populated, leading to a redistribution of the spin population and a subsequent decrease in magnetization. Indeed, the rate of change of the population of the excited level under optical pumping, neglecting stimulated emission, is given by the general rate equation $dN/dt = R_P(N - N_0) - (N/T_1)$, where $N_0$ is the maximum possible number of centers involved, $R_P$ is the pumping rate and $1/T_1$ is the spontaneous emission rate.[113] Under continuous light irradiation, a steady state is reached ($dN/dt$ = 0), such that the ratio between centers in the excited and ground state is $N/N_0 = R_P T_1/(1 + R_P T_1)$. Therefore, for processes such that the pumping rate is larger than the deexcitation rate, a population inversion can be obtained.

The maximum expected change of magnetization, if the excited state could be fully populated, has been calculated by *ab initio*, yielding $\Delta M^{max}$ = 0.95–0.43$\mu_B$ = 0.52$\mu_B$ at $T$ = 1.8 K under 1 kOe. However, continuous optical pumping, coupled with the efficiency of sensitization and desexcitation rates, is expected to result in a partial population distribution between the excited and ground states, diminishing the effect. The observed light-induced magnetization change, $\Delta M$(off/on) =

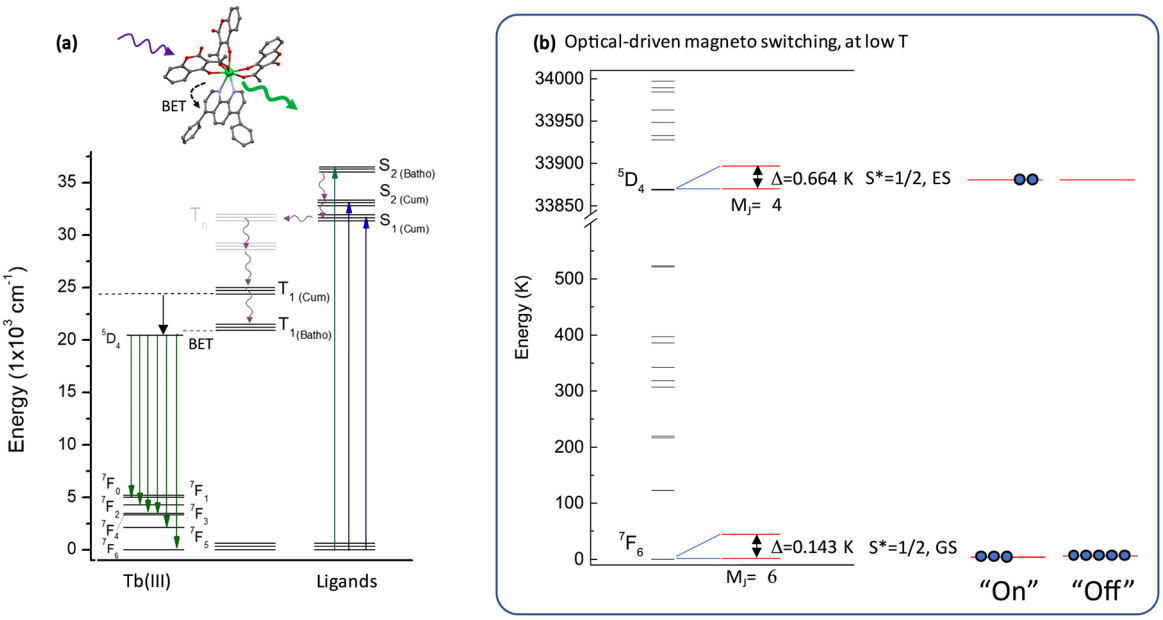


Fig. 6 (a) Energy level scheme and energy transfer mechanism in **Tb–batho**, at room *T*; (b) *ab initio* calculated energy levels, highlighting the energy splitting of the ground and optically-excited states quasi-doublets, and proposed mechanism for optical-driven magneto-switching observed at low *T*.

$0.376\mu_B$ fu$^{-1}$ at 1.8 K (pellet 1), being lower than the maximum possible value, $\Delta M^{max}$, suggests that the excited population reaches, at most, 72%. The reduction of this effect at high magnetic fields, as observed in Fig. 3(b), may be explained by the decrease in spontaneous emission due to the Zeeman effect.[114,115]

We postulate that the above mechanism is occurring in this system and may explain the observed behavior. However, although no temperature variation is detected by the thermometer located next to the sample (Fig. 2(d)), we cannot completely exclude a small change in local temperature associated with energy absorption by the molecule and non-radiative de-excitation. Further research could focus on improving the pumping process to enhance the observed light-induced magnetic modulation for potential applications.

## 4. Conclusions

In summary, our study reveals the intriguing magneto-optical properties of a versatile multifunctional Tb complex, incorporating coumarin as main antenna and batho as ancillary ligand, which combines SIM behavior, high quantum yield luminescence in the visible, and reversible light-induced magnetic switching. The observed decrease of the magnetization upon light irradiation is most prominent when exciting the "antenna" ligands at 380 nm, resulting in an "off/on" magnetization change of $\Delta M$(off/on) = $0.376\mu_B$ fu$^{-1}$ (that is, *ca.* 42.6% of the magnetization) at 1.8 K and 1 kOe. This optical-induced effect may be explained by a spin population redistribution between the $M_J$ = 4 excited state and $M_J$ = 6 ground state. The capability to control magnetization states through optical stimulation, toggling between an "on" and "off" state, presents an appealing feature. This property opens up diverse possibilities for the development of molecular nanomaterials, with potential application in advanced electronic devices *e.g.* for switching, sensors, or quantum computing.

## Author contributions

EB: conceptualization, supervision, funding acquisition, resources, investigation, formal analysis, data curation, visualization, writing – original draft, review and edit; AA: conceptualization, supervision, investigation, formal analysis, writing – review; JL: investigation, writing – review (*ab initio* calculations); LG: resources, investigation, writing – review (synthesis of sample).

## Data availability

Further data supporting this article have been included as part of the ESI.† Crystallographic data for **Tb–batho** is deposited at the CCDC repository under 2013258.

## Conflicts of interest

There are no conflicts to declare.

## Acknowledgements

This work was financially supported by the Spanish "Ministerio de Ciencia, Innovacion y Universidades" (PID2022-138492NB-I00), the Gobierno de Aragón (RASMIA E12-23R), the State Investigation Agency, through the Severo Ochoa Programme for Centres of Excellence in R&D (CEX2023-001263-S and CEX2023-001286-S), and Mexican PAPIIT program (IN219321).

 

Authors would like to acknowledge the use of Servicio General de Apoyo a la Investigación-SAI, Universidad de Zaragoza.

## References

1 L. Bogani and W. Wernsdorfer, *Nat. Mater.*, 2008, **7**, 179–186.
2 P. Dechambenoit and J. R. Long, *Chem. Soc. Rev.*, 2011, **40**, 3249–3265.
3 B. Li, H.-M. Wen, Y. Cui, W. Zhou, G. Qian and B. Chen, *Adv. Mater.*, 2016, **28**, 8819–8860.
4 P. Horcajada, R. Gref, T. Baati, P. K. Allan, G. Maurin, P. Couvreur, G. Férey, R. E. Morris and C. Serre, *Chem. Rev.*, 2012, **112**, 1232–1268.
5 J. Long, Y. Guari, C. Guerin and J. Larionova, *Dalton Trans.*, 2016, **45**, 17581–17587.
6 J. Long, G. Yannick, R. A. S. Ferreira, L. D. Carlos and J. Larionova, *Coord. Chem. Rev.*, 2018, **363**, 57–70.
7 A. Shevchenko, M. Korppi, K. Lindfors, M. Heiliö, M. Kaivola, E. Il'yashenko and T. H. Johansen, *Appl. Phys. Lett.*, 2007, **91**, 041916.
8 S. Manz, M. Matsubara, T. Lottermoser, J. Büchi, A. Iyama, T. Kimura, D. Meier and M. Fiebig, *Nat. Photonics*, 2016, **10**, 653–656.
9 Y. Einaga, *J. Photochem. Photobiol., C*, 2006, **7**, 69–88.
10 M. Khela, M. Dąbrowski, S. Khan, P. S. Keatley, I. Verzhbitskiy, G. Eda, R. J. Hicken, H. Kurebayashi and E. J. G. Santos, *Nat. Commun.*, 2023, **14**, 1378.
11 R. Sessoli and A. K. Powell, *Coord. Chem. Rev.*, 2009, **253**, 2328–2341.
12 R. A. Layfield and M. Murugesu, *Lanthanides and actinides in Molecular magnetism*, Wiley-VCH, 2015.
13 E. Bartolomé, A. Arauzo, J. Luzón, J. Bartolomé and F. Bartolomé, in *Handbook of Magnetic Materials*, ed. E. Brück, Elsevier, 2017, pp. 1–289.
14 F. S. Guo, B. M. Day, Y. C. Chen, M. L. Tong, A. Mansikkamäki and R. A. Layfield, *Science*, 2018, **362**, 1400–1403.
15 J.-C. G. Bünzli and C. Piguet, *Chem. Soc. Rev.*, 2005, **34**, 1048–1077.
16 *Molecular Magnetic Materials*, ed. B. Sieklucka and D. Pinkowicz, Wiley-VCH Verlag GmbH, Weinheim, Germany, 2017.
17 S. V. Eliseeva and J.-C. G. Bünzli, *Chem. Soc. Rev.*, 2010, **39**, 189–227.
18 D. Prodius and A.-V. Mudring, *Coord. Chem. Rev.*, 2018, **363**, 1–16.
19 J. Long, I. V. Basalov, N. V. Forosenko, K. A. Lyssenko, E. Mamontova, A. V. Cherkasov, M. Damjanović, L. F. Chibotaru, Y. Guari, J. Larionova and A. A. Trifonov, *Chem. – Eur. J.*, 2019, **25**, 474–478.
20 E. Mamontova, J. Long, R. A. S. Ferreira, A. M. P. Botas, D. Luneau, Y. Guari, L. D. Carlos and J. Larionova, *Magnetochemistry*, 2016, **2**, 41.
21 M. Gregson, N. F. Chilton, A.-M. Ariciu, F. Tuna, I. F. Crowe, W. Lewis, A. J. Blake, D. Collison, E. J. L. McInnes, R. E. P. Winpenny and S. T. Liddle, *Chem. Sci.*, 2016, **7**, 155–165.
22 J. Jung, T. T. da Cunha, B. Le Gennic, F. Pointillart, C. L. M. Pereira, J. Luzon, S. G. Lahcène, O. Cador, L. Ouahab and O. Maury, *Eur. J. Inorg. Chem.*, 2014, 3888–3894.
23 H.-R. Wen, J.-L. Zhang, F.-Y. Liang, K. Yang, S.-J. Liu, J.-S. Liao and C.-M. Liu, *New J. Chem.*, 2019, **43**, 4067–4074.
24 S. Shintoyo, K. Murakami, F. Takeshi, N. Matsumoto, N. Mochida, T. Ishida, Y. Sunatsuki, M. Watanabe, M. Tsuchimoto, J. Mrozinski, C. Coletti and N. Re, *Inorg. Chem.*, 2014, **53**, 10359–10369.
25 F. Guégan, J. Jung, B. Le Guennic, F. Riobé, O. Maury, B. Gillon, J.-F. Jacquot, Y. Guyot, C. Morell and D. Luneau, *Inorg. Chem. Front.*, 2019, **6**, 3152–3157.
26 G. Brunet, R. Marin, M.-J. Monk, U. Resch-Genger, D. A. Gálico, F. A. Sigoli, E. A. Suturina, E. Hemmer and M. Murugesu, *Chem. Sci.*, 2019, **10**, 6799–6808.
27 P. P. Svetlana, A. B.Ilyukhina, A. V.Gavrikova, Y. A. Mikhlina, L. N. Puntus, E. Varaksina and N. M. Novototrtseva, *Inorg. Chim. Acta*, 2019, **486**, 499–505.
28 S. Chorazy, M. Zychowicz, S. I. Ohkoshi and B. Sieklucka, *Inorg. Chem.*, 2019, **58**, 165–179.
29 X.-H. Lv, S.-L. Yang, Y.-X. Li, C.-X. Zhang and Q.-L. Wang, *RSC Adv.*, 2017, **7**, 38179–38186.
30 J.-R. Jimenez, I. Diaz-Ortega, E. Ruiz and E. Al, *Chem. – Eur. J.*, 2016, **22**, 14548–14559.
31 L. Mandal, S. Biswas and M. Yamashita, *Magnetochemistry*, 2019, **169**, 187–194.
32 D. Errulat, R. Marin, D. A. Gálico, K. L. M. Harriman, A. Pialat, B. Gabidullin, F. Iikawa, O. D. D. Couto, J. O. Moilanen, E. Hemmer, F. A. Sigoli, M. Murugesu, O. D. D. Couto, J. O. Moilanen, E. Hemmer, F. A. Sigoli and M. Murugesu, *ACS Cent. Sci.*, 2019, **5**, 1187–1198.
33 N. Yao-Yao, W. Wen-Min, C. Xiao-Ya, C. Hong-Man, H. ShaoXia, L. Zhen, C. Jian-Zhong and G. Hong-Ling, *Polyhedron*, 2018, **42**, 11417–11429.
34 B. Casanovas, M. Font-Bardía, S. Speed, M. S. El Fallah and R. Vicente, *Eur. J. Inorg. Chem.*, 2018, 1928–1937.
35 Q. Shuiling, Z. Jun, Z. Sheng, Y. Qi, W. Qin, Y. Desuo and C. Sanping, *New J. Chem.*, 2017, **41**, 5467–5475.
36 S. Gui-Fang, Z. Cong-Ming, G. Jian-Ni, Y. Meng and L. Li-Cun, *J. Mol. Struct.*, 2017, **1135**, 106–111.
37 O. Sun, P. Chen, H.-F. Li, T. Gao, W.-B. Sun, G.-M. Li and P.-F. Yan, *CrystEngComm*, 2016, **18**, 4627–4635.
38 H.-Y. Shen, W.-M. Wang, H.-L. Gao and J.-Z. Cui, *RSC Adv.*, 2016, **6**, 34165–34174.
39 H.-Y. Shen, W.-M. Wang, Y.-X. Bi, H.-L. Gao, S. Liub and J.-Z. Cui, *Dalton Trans.*, 2015, **44**, 18893–18901.
40 H. Min, H. Zhao, C. Sañudo and M. Chen, *Polyhedron*, 2015, **101**, 270–275.
41 M. Pengtao, W. Rong, S. Yanan, H. Feng, W. Yueyan, N. Jingyang and W. Jingping, *Dalton Trans.*, 2015, **44**, 11514–11523.
42 W. Wen-Min, Z. Li, L. Xian-Zhen, H. Li-Yuan, W. Xin-Xin, S. Ying, J. Wang, J. Dong and Z.-L. Wu, *New J. Chem.*, 2019, **43**, 12941–12949.

43 W. Qing-Li, W. Ru-Fen, C. Chun-Zhu, Y. Rong-Xin, G. Yu, S. Peng-Fei and W. Wen-Min, *Polyhedron*, 2018, **50**, 92–96.
44 Q. Yaru, G. Yu, Z. Shasha, S. Hao, J. Yu and Y. Li, *RSC Adv.*, 2018, **8**, 12641–12652.
45 H. H. Zou, R. Wang, Z. L. Chen, D. C. Liu and F. P. Liang, *Dalton Trans.*, 2014, **43**, 2581–2587.
46 Y.-H. Chen, Y.-F. Tsai, G.-H. Lee and E.-C. Yang, *J. Solid State Chem.*, 2012, **185**, 166–171.
47 A. B. Ruiz-Muelle, A. García-García, A. A. García-Valdivia, I. Oyarzabal, J. Cepeda, J. M. Seco, E. Colacio, A. Rodríguez-Diéguez and I. Fernández, *Dalton Trans.*, 2018, **47**, 12783–12794.
48 E. Bartolomé, J. Bartolomé, A. Arauzo, J. Luzón, R. Cases, S. Fuertes, V. Sicilia, A. I. Sánchez-Cano, J. Aporta, S. Melnic, D. Prodius and S. Shova, *J. Mater. Chem. C*, 2018, **6**, 5286–5299.
49 W.-H. Zhu, X. Xiong, C. Gao, S. Li, Y. Zhang, J. Wang, C. Zhang, A. K. Powell and S. Gao, *Dalton Trans.*, 2017, **46**, 14114–14121.
50 M. Al Hareri, Z. R. Ali, J. Regier, E. L. Gavey, L. D. Carlos, R. A. S. Ferreira and M. Pikington, *Inorg. Chem.*, 2017, **56**, 7344–7353.
51 X.-L. Li, C.-L. Chen, H.-P. Xiao, A.-L. Wang, C.-M. Liu, X. Zheng, L.-J. Gao, X.-G. Yanga and S.-M. Fang, *Dalton Trans.*, 2013, **42**, 15317–15325.
52 D. T. Thielemann, M. Klinger, T. J. A. Wolf, Y. Lan, W. Wernsdorfer, M. Busse, P. W. Roesky, A.-N. Unterreiner, A. K. Powell, P. C. Junk and G. B. Deacon, *Inorg. Chem.*, 2011, **50**, 11990–12000.
53 Y. Jia, H. Li, P. Chen, T. Gao, W. Sun and P. Yan, *Aust. J. Chem.*, 2018, **71**, 527–533.
54 E. Bartolomé, A. Arauzo, S. Fuertes, L. Navarro-Spreafica, P. Sevilla, H. F. Cortés, N. Settineri, S. J. Teat and E. C. Sañudo, *Dalton Trans.*, 2023, **52**, 7258–7270.
55 Z. Li, X.-B. Li, M. E. Light, A. E. Carrillo, A. Arauzo, M. Valvidares, C. Roscini, F. Teixidor, C. Viñas, F. Gándara, E. Bartolomé and J. G. Planas, *Adv. Funct. Mater.*, 2023, **33**, 2307369.
56 R. Marin, G. Brunet and M. Murugesu, *Angew. Chem., Int. Ed.*, 2021, **60**, 1728–1746.
57 J. Long, *Front. Chem.*, 2019, **7**, 1–7.
58 J. Jian-Hua, L. Quan-Wen, C. Yan-Cong, L. Jun-Liang and T. Ming-Liang, *Coord. Chem. Rev.*, 2019, **378**, 365–381.
59 M. Latva, H. Takalo, V.-M. Mukkala, C. Matachescu, J. C. Rodríguez-Ubis and J. Kankare, *J. Lumin.*, 1997, **75**, 149–169.
60 Y. Bi, X.-T. Wang, W. Liao, X. Wang, R. Deng, H. Zhang and S. Gao, *Inorg. Chem.*, 2009, **48**, 11743–11747.
61 J. Long, Y. Guari, R. A. S. Ferreira, L. D. Carlos and J. Larionova, *Coord. Chem. Rev.*, 2018, **363**, 57–70.
62 J.-H. Jia, Q.-W. Li, Y.-C. Chen, J.-L. Liu and M.-L. Tong, *Coord. Chem. Rev.*, 2019, **378**, 365–381.
63 Y. Xin, J. Wang, M. Zychowicz, J. J. Zakrzewski, K. Nakabayashi, B. Sieklucka, S. Chorazy and S. I. Ohkoshi, *J. Am. Chem. Soc.*, 2019, **141**, 18211–18220.
64 J. L. Liu, Y. C. Chen, Y. Z. Zheng, W. Q. Lin, L. Ungur, W. Wernsdorfer, L. F. Chibotaru and M. L. Tong, *Chem. Sci.*, 2013, **4**, 3310–3316.
65 Q. Zhou, F. Yang, B. Xin, G. Zeng, X. Zhou, K. Liu, D. Ma, G. Li, Z. Shi and S. Fenga, *Chem. Commun.*, 2013, **49**, 8244–8246.
66 X. Zhang, V. Vieru, X. Feng, J.-L. Liu, Z. Zhang, B. Na, W. Shi, B.-W. Wang, A. K. Powell, L. F. Chibotaru, S. Gao, P. Cheng and J. R. Long, *Angew. Chem., Int. Ed.*, 2015, **54**, 9861–9865.
67 J. Y. Ge, L. Cui, J. Li, F. Yu, Y. Song, Y. Q. Zhang, J. L. Zuo and M. Kurmoo, *Inorg. Chem.*, 2017, **56**, 336–343.
68 D. Tanaka, T. Inose, H. Tanaka, S. Lee, N. Ishikawa and T. Ogawa, *Chem. Commun.*, 2012, **48**, 7796–7798.
69 K. Suzuki, R. Sato and N. Mizuno, *Chem. Sci.*, 2013, **4**, 596–600.
70 Z. Liang, M. Damjanović, M. Kamila, G. Cosquer, B. K. Breedlove, M. Enders and M. Yamashita, *Inorg. Chem.*, 2017, **56**, 6512–6521.
71 P. Zhang, M. Perfetti, M. Kern, P. P. Hallmen, L. Ungur, S. Lenz, M. R. Ringenberg, W. Frey, H. Stoll, G. Rauhut and J. Van Slageren, *Chem. Sci.*, 2018, **9**, 1221–1230.
72 B. S. Dolinar, S. Gómez-Coca, D. I. Alexandropoulos and K. R. Dunbar, *Chem. Commun.*, 2017, **53**, 2283–2286.
73 S. Takamatsu, T. Ishikawa, S. Y. Koshihara and N. Ishikawa, *Inorg. Chem.*, 2007, **46**, 7250–7252.
74 M. Gonidec, E. S. Davies, J. McMaster, D. B. Amabilino and J. Veciana, *J. Am. Chem. Soc.*, 2010, **132**, 1756–1757.
75 L. Norel, M. Feng, K. Bernot, T. Roisnel, T. Guizouarn, K. Costuas and S. Rigaut, *Inorg. Chem.*, 2014, **53**, 2361–2363.
76 C. M. Dickie, A. L. Laughlin, J. D. Wofford, N. S. Bhuvanesh and M. Nippe, *Chem. Sci.*, 2017, **8**, 8039–8049.
77 D. Pinkowicz, M. Ren, L.-M. Zheng, S. Sato, M. Hasegawa, M. Morimoto, M. Irie, B. K. Breedlove, G. Cosquer, K. Yamashita and M. Katoh, *Chem. – Eur. J.*, 2014, **20**, 12502–12513.
78 L. F. Wang, J. Z. Qiu, J. L. Liu, Y. C. Chen, J. H. Jia, J. Jover, E. Ruiz and M. L. Tong, *Chem. Commun.*, 2015, **51**, 15358–15361.
79 L. F. Wang, J. Z. Qiu, Y. C. Chen, J. L. Liu, Q. W. Li, J. H. Jia and M. L. Tong, *Inorg. Chem. Front.*, 2017, **4**, 1311–1318.
80 J. Li, M. Kong, L. Yin, J. Zhang, F. Yu, Z. W. Ouyang, Z. Wang, Y. Q. Zhang and Y. Song, *Inorg. Chem.*, 2019, **58**, 14440–14448.
81 P. Selvanathan, V. Dorcet, T. Roisnel, K. Bernot, G. Huang, B. Le Guennic, L. Norel and S. Rigaut, *Dalton Trans.*, 2018, **47**, 4139.
82 M. Hojorat, H. Al Sabea, L. Norel, K. Bernot, T. Roisnel, F. Gendron, B. Le Guennic, E. Trzop, E. Collet, J. R. Long and S. Rigaut, *J. Am. Chem. Soc.*, 2020, **142**, 931–936.
83 Y. J. Ma, J. X. Hu, S. De Han, J. Pan, J. H. Li and G. M. Wang, *J. Am. Chem. Soc.*, 2020, **142**, 2682–2689.
84 X. Da Huang, Y. Xu, K. Fan, S. S. Bao, M. Kurmoo and L. M. Zheng, *Angew. Chem., Int. Ed.*, 2018, **57**, 8577–8581.

 

85 S. L. Bayliss, D. W. Laorenza, P. J. Mintun, B. D. Kovos, D. E. Freedman and D. D. Awschalom, *Science*, 2020, **370**, 1309–1312.
86 K. S. Kumar, D. Serrano, A. M. Nonat, B. Heinrich, L. Karmazin, L. J. Charbonnière, P. Goldner and M. Ruben, *Nat. Commun.*, 2021, 2152.
87 E. Moreno-Pineda and W. Wernsdorfer, *Nat. Rev.*, 2020, 1309.
88 O. Guzmán-Méndez, F. González, S. Bernès, M. Flores-Álamo, J. Ordóñez-Hernández, H. García-Ortega, J. Guerrero, N. Aliaga-Alcalde, W. Qian and L. Gasque, *Inorg. Chem.*, 2018, **57**, 908–911.
89 Q. Ma, Y. Zheng, N. Armaroli, M. Bolognesi and G. Accorsi, *Inorg. Chim. Acta*, 2009, **362**, 3181–3186.
90 X. Yi, K. Bernot, F. Pointillart, G. Poneti, G. Calvez, C. Daiguebonne, O. Guillou and R. Sessoli, *Chemistry*, 2012, **18**, 11379–11387.
91 W. Chu, Q. Sun, P. Y. Xu Yao, G. An and G. Li, *RSC Adv.*, 2015, **5**, 94802–94808.
92 K. Yamashita, R. Miyazaki, Y. Kataoka, T. Nakanishi, Y. Hasegawa, M. Nakano, T. Yamamura and T. Kajiwara, *Dalton Trans.*, 2013, **42**, 1987–1990.
93 S. Yamauchi, T. Fujinami, N. Matsumoto, N. Mochida, T. Ishida, Y. Sunatsuki, M. Watanabe, M. Tsuchimoto, C. Coletti and N. Re, *Inorg. Chem.*, 2014, **53**, 5961–5971.
94 High Power Tuneable Light Source (280–1100 nm) TLS120Xe, **https://qd-europe.com/es/en/news/latest-updates/newsdetails/high-power-tuneable-light-source-280-nm-1100-nm-tls120xe–1820/**.
95 B. O. Roos and P. A. Malmqvist, *Phys. Chem. Chem. Phys.*, 2004, **6**, 2919.
96 F. Aquilante, L. de Vico, N. Ferré, G. Ghigo, P.-Å. Malmqvist, P. Neogrády, T. Pedersen, M. Pitonák, M. Reiher, B. O. Roos, L. Serrano-Andrés, M. Urban, V. Verzayov and R. Lindh, *J. Comput. Chem.*, 2010, **31**, 224–247.
97 B. O. Roos, R. Lindh, P. A. Malmqvist, V. Veryazov and P.-O. Widmark, *J. Phys. Chem. A*, 2004, **108**, 2851.
98 A. Arauzo, L. Gasque, S. Fuertes, C. Tenorio, S. Bernès and E. Bartolomé, *Dalton Trans.*, 2020, **49**, 13671–13684.
99 *Nomenclature of Inorganic Chemistry*, ed. N. G. Connelly, T. Damhus, R. M. Hartshorn and A. T. Hutton, IUPAC Recommendations 2005 (IUPAC Red Book), RSC Publishing, 2005.
100 A. Abragam and B. Bleaney, *Electron Paramagnetic Resonance of Transition Ions*, 1970, pp. 4, 42, 133–163, 398–406, 417–430, 541–547, 583–599.
101 SQUID Magnetometer Quantum Design MPMS®3, **https://www.qdusa.com/products/mpms3.html#productOptions**, (accessed 27 July 2023).
102 E. Bartolomé, J. Bartolomé, S. Melnic, D. Prodius, S. Shova, A. Arauzo, J. Luzón, F. Luis and C. Turta, *Dalton Trans.*, 2013, **42**, 10153–10171.
103 E. Bartolomé, J. Bartolomé, S. Melnic, D. Prodius, S. Shova, A. Arauzo, J. Luzón, L. Badía-Romano, F. Luis and C. Turta, *Dalton Trans.*, 2014, **43**, 10999–11013.
104 E. Bartolomé, J. Bartolomé, A. Arauzo, J. Luzón, L. Badía, R. Cases, F. Luis, S. Melnic, D. Prodius, S. Shova and C. Turta, *J. Mater. Chem. C*, 2016, **4**, 5038–5050.
105 E. Bartolomé, A. Arauzo, J. Luzón, S. Melnic, S. Shova, D. Prodius, J. Bartolomé, A. Amanne, M. Nallaiyane and S. Spagna, *Dalton Trans.*, 2019, **48**, 5022–5034.
106 E. Bartolomé, A. Arauzo, J. Luzón, S. Melnic, S. Shova, D. Prodius, I. C. Nlebedim, J. Bartolomé and F. Bartolomé, *Dalton Trans.*, 2019, **48**, 15386–15396.
107 J. González, P. Sevilla, G. Gabarró-Riera, J. Jover, J. Echeverría, S. Fuertes, A. Arauzo, E. Bartolomé and E. C. Sañudo, *Angew. Chem., Int. Ed.*, 2021, **60**, 12001–12006.
108 G. J. Gerritsma, J. Flokstra, G. A. Hartemink, J. J. M. Scholten, A. J. W. A. Vermeulen and L. C. van der Marel, *Phys. B&C*, 1978, **95**, 173–182.
109 J. A. Overweg, J. Flokstra and G. J. Gerritsma, *Physica*, 1982, **112B**, 381–388.
110 J. Flokstra, G. J. Gerritsma, G. A. Hartemink and L. C. van der Marel, *Physica*, 1974, **77**, 99–120.
111 J. Flokstra, G. J. Gerritsma and L. C. van der Marel, *Physica*, 1977, **92B**, 350.
112 J. S. Griffith, *Phys. Rev.*, 1963, **132**, 316–319.
113 B. Di Bartolo, *Optical interactions in solids*, J. Wiley, New York, 1968.
114 U. V. Valiev, D. R. Dzhuraev, S. I. Mukhamedkhanova, N. M. Narzullaev, V. Y. Sokolov and S. A. Rakhimov, *Russ. Phys. J.*, 2008, **51**, 593–600.
115 Y. Bi, C. Chen, Y. F. Zhao, Y. Q. Zhang, S. Da Jiang, B. W. Wang, J. B. Han, J. L. Sun, Z. Q. Bian, Z. M. Wang and S. Gao, *Chem. Sci.*, 2016, **7**, 5020–5031.